

# SET Pulse-Width Measurement Eliminating Pulse-Width Modulation and Within-die Process Variation Effects

Ryo Harada<sup>†</sup> Yukio Mitsuyama<sup>‡</sup> Masanori Hashimoto<sup>†</sup> Takao Onoye<sup>†</sup>

<sup>†</sup>Dept. Information Systems Engineering, Osaka University, Japan & JST CREST

<sup>‡</sup>School of Systems Engineering, Kochi University of Technology, Japan & JST CREST

**Abstract**—This paper presents a measurement circuit structure for capturing SET pulse-width suppressing pulse-width modulation and within-die process variation effects. For mitigating pulse-width modulation while maintaining area efficiency, the proposed circuit uses massively parallelized short inverter chains as a target circuit. Moreover, for each inverter chain on each die, pulse-width calibration is performed. In measurements, narrow SET pulses ranging 5 ps to 215 ps were obtained. We confirm that an overestimation of pulse-width may happen when ignoring die-to-die and within-die variation of the measurement circuit. Our evaluation results thus point out that calibration for within-die variation in addition to die-to-die variation of the measurement circuit is indispensable.

## I. INTRODUCTION

As circuit integration advances to a very large scale, neutron induced soft error is becoming an actual concern even at sea level. Especially in combinational logic, single event transient (SET) is a threat to degrade circuit reliability. After propagating through several combinational logic gates, a neutron-induced SET pulse finally arrives at a memory element and may be captured depending on the pulse-width and clock timing [1]. Therefore, it is important for calculation of SET-induced error rate to characterize the probability distribution of SET pulse-width.

Recently, several measurement circuits for obtaining SET pulse-width have been proposed. Figure 1 shows a popular SET measurement structure with a pulse-width measurement circuit. It is implemented on a chip with a target circuit where SETs are expected to occur, which is often realized by a combinational gate chain. On the other hand, because of limited radiation time, area efficient implementation of measurement and target circuit is necessary. For this purpose, conventional measurements often adopted a very long gate chain as a target circuit to increase the area ratio of the target circuit to the measurement circuit. However, such a long combinational chain involves pulse-width variation due to propagation induced pulse broadening (PIPB) [2] and mismatch between rise and fall delays [3], which may excessively increase the pulse-width or vanish the pulse itself. In this case, the measured pulse-width distribution becomes totally different from that in actual circuits.

Furthermore, process variation fluctuates the performance of measurement circuit. As technology advances, within-die process variation becomes significant, which means measurement circuits even on the same die do not have the same performance, especially in low voltage operation.

In this work, to overcome the above pulse-width modulation while maintaining area efficiency, we present a measure-

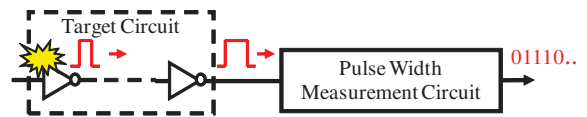


Fig. 1. Popular SET measurement structure. SET pulse-width may be modulated in target circuit.

ment circuit structure with parallelized shallow inverter chains. We introduced OR cones to converge the outputs of the inverter chains into a pulse-width measurement circuit. In addition, for calibrating within-die performance variation and performance mismatch of measurement circuit including the converging paths, we embed a calibration circuit that can exercise each chain and obtain the response of pulse-width measurement circuit. We confirm that the proposed structure can achieve higher area efficiency by increasing the number of parallelized chains. Experimental results of neutron radiation tests using 65nm test chips show that the SET pulse-widths observed in our 512-parallelized 10-stage inverter chains are statistically narrower than results previously reported using a long combinational chain. Calibration results indicate that pulse-width distribution may be overestimated when die-to-die and within-die variations of the measurement circuit are not considered. Calibration results also show that the response of measurement circuit is influenced by not only die-to-die variation but also within-die variation, and clearly point out the importance of within-die variation elimination.

The remainder of this paper is organized as follows. Section II introduces the proposed measurement structure. Section III presents the radiation experimental results and calibration results of test chip. Section IV discusses the impact of variation in the measurement circuit on SET pulse-width measurements. Section V concludes this paper.

## II. PROPOSED MEASUREMENT STRUCTURE

Figure 2 illustrates the proposed circuit structure for measurement. We use parallelized inverter chains as a target circuit and bundle them to a single pulse-width measurement circuit. Similar parallelization is found in [4]. Using this structure, while we can suppress the pulse-width modulation by using short inverter chains, we can increase the area ratio of the target circuit to the measurement circuit. Among circuits previously proposed for pulse-width measurement, we select a two-stage measurement circuit that consists of a pulse-to-time converter and a time-to-digital converter [5]. In this work, Vernier delay line (VDL) is used as the time-to-digital converter.

VDL is composed of two buffer chains and a D-type latch

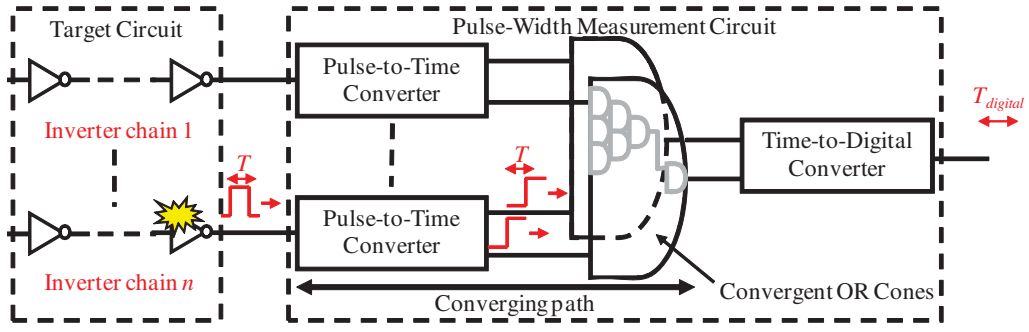


Fig. 2. Proposed circuit structure for SET pulse-width measurement.

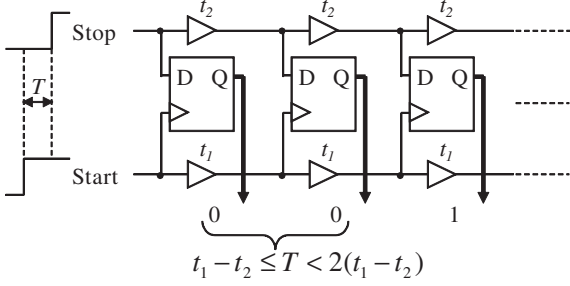


Fig. 3. Circuit configuration of Vernier delay line. The case of  $N = 2$  is shown.

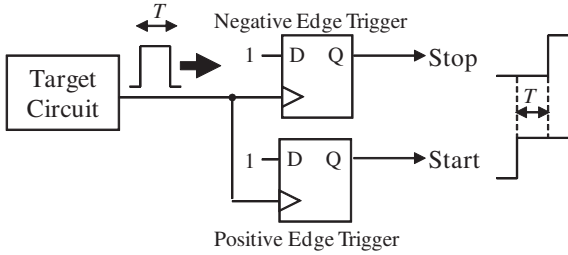


Fig. 4. Pulse-to-time converter consisting of two D-FFs of positive and negative edge trigger.

chain, as illustrated in Figure 3. Two step signals (START and STOP) with  $T$  time difference are given to this circuit, and  $T$  is to be measured by VDL. The buffer delay of the chain for START signal  $t_1$  is larger than that for STOP  $t_2$ . START chain gives clock signals and STOP chain provides data signals to latches. START and STOP signals race and finally STOP signal overtakes START signal. When START and STOP signals propagate through a single stage, the time difference between them, which was initially  $T$  at the input, is reduced by  $t_r = (t_1 - t_2)$ . Latches at which the time difference becomes 0 or below store 1 and the others latch 0. Letting  $N$  denote the number of latches storing 0, the time difference  $T$  is estimated by

$$(N - 1)t_r \leq T + t_s < Nt_r, \quad (1)$$

where  $t_s$  is the setup time of a latch.

Figure 4 shows the circuit configuration of the pulse-to-time converter. The output of the lower FF first changes from low to high at the rising edge of SET pulse, and subsequently that of the upper FF transitions at the falling edge. Thus, START and STOP signals with  $T$  time interval are generated.

Using these circuits, an SET is first converted to two step signals whose interval is equal to SET pulse-width  $T$  as shown in Figure 2, and then the time interval  $T$  is digitalized by VDL. For guiding SETs occurring in parallelized chains into the VDL, we insert two convergent cones of OR gates for the first and second step signals between the target circuit and VDL. Note that while SETs generated in the target circuit trigger VDL, an SET invoked inside one of the OR cones delivers only a single step signal to VDL and hence cannot trigger VDL, which means SETs of OR gates are discarded. Hereafter, the path between the output of target circuit and VDL is called converging path.

To obtain a precise SET pulse-width distribution by overcoming within-die and die-to-die variations of the measurement circuit, the following two requirements must be satisfied.

*R1: chain-by-chain pulse-width calibration*

We need to calibrate the fluctuation of VDL time resolution and the performance mismatch among the converging paths.

*R2: indication of a chain where an SET occurs*

To apply an appropriate calibration result, we need to know where the observed SET occurred.

Figure 5 explains the proposed calibration scheme for each inverter chain to satisfy *R1*. An on-chip pulse generator injects a pseudo SET pulse whose width can be precisely tuned into the output of inverter chain and its width is measured in VDL. The chain selector determines the inverter chain where a pseudo SET is injected. The on-chip pulse generator needs to satisfy; 1) the time resolution of pulse-width is finer than that of VDL, 2) the pulse-width range that can be generated covers SET pulse and VDL time ranges, and 3) the generated pulse-width can be assessed in another way.

The on-chip pulse generator used for the implementation is mainly composed of an XOR gate, selectable delay elements, and a bit counter. In this circuit, an input transition is converted into a pulse whose pulse-width is equal to the propagation delay of the delay element ( $t_{d1}$ ) as shown Figure 6(a). By selecting a delay element and adjusting its power supply voltage, we can continuously change the pulse-width, which means 1) and 2) are satisfied.

Meanwhile,  $t_{d1}$  is influenced by manufacturing variability, and then  $t_{d1}$  should be measured after fabrication to assess the width of the generated pulse. The assessment process of delay element is explained in the following. The oscillating period of the path without delay element (Figure 6(b)) is calculated from

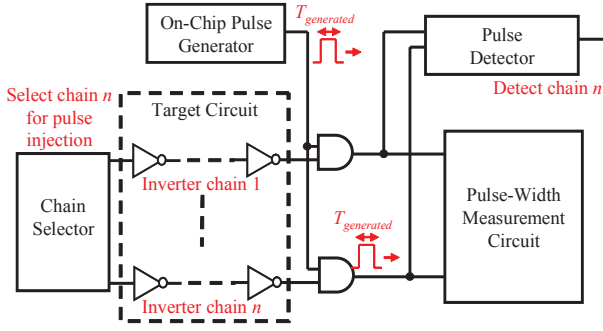


Fig. 5. Proposed calibration scheme for each inverter chain.

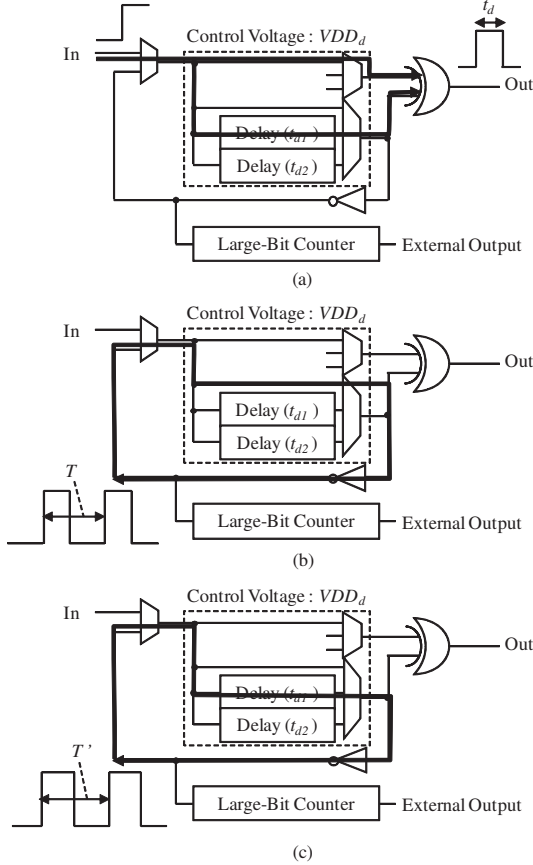


Fig. 6. Schematic and operation examples of on-chip pulse generator: (a) pulse generation with  $t_{d1}$  width, (b) oscillation using the path without delay circuit, and (c) oscillation using the path including  $t_{d1}$ .

the counts in the large-bit counter while it is configured to oscillate. Similarly, the oscillating period of the path including  $t_{d1}$  (Figure 6(c)) is calculated. Based on these two oscillating periods, we can obtain  $t_{d1}$ . This satisfies 3).

Besides, to identify and record the inverter chain where an SET occurs, i.e. for R2, we add a pulse detector to the output of each inverter chain. Based on the VDL outputs obtained in the calibration for the inverter chain where an SET occurs under radiation, we can compute the pulse-width at the output of the target circuit. With this procedure, the performance mismatch of the converging paths and the variation of VDL time resolution due to within-die and die-to-die variations can be eliminated. Note that the mismatch of the converging paths is also caused

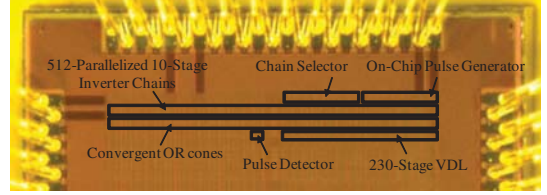


Fig. 7. A micrograph of the test chip in a 65 nm process. The sensitive area of the target circuit is about  $805 \mu\text{m}^2$ .

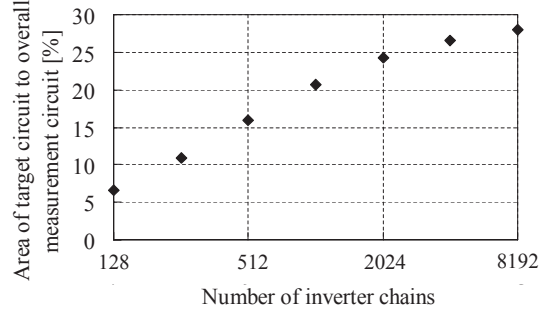


Fig. 8. Area ratio of target circuit to overall measurement circuit.

by design difference due to, for example, wire length difference in addition to within-die variation. On the other hand, the presented procedure can eliminate both of them, though the design difference will not be explicitly discussed in the rest of this paper.

### III. RADIATION EXPERIMENT AND CALIBRATION

To confirm the operation of the proposed circuit, a test chip was fabricated in 65 nm process. A micrograph of the test chip is shown in Figure 7. The test circuit is composed of 512-parallelized 10-stage inverter chains, 230-stage VDL, and other calibration circuits. Inverters of standard size are used for inverter chains and tap cells are placed in  $10 \mu\text{m}$  interval. This 230-stage VDL was designed to achieve 4.8 ps time resolution. In this implementation, larger-sized buffers are used for VDL to suppress the within-die variation. It is 12 times larger than the standard buffer.

Figure 8 shows the area ratio of target circuit to overall measurement circuit when the number of inverter chains in parallel is varied. Here, the overall measurement circuit includes all the circuits necessary for measurement including target, pulse-width measurement, and calibration circuits. The area ratio of the test chip configuration is 16 %, and we can raise it by increasing the number of inverter chains in parallel.

Neutron radiation tests were performed at Research Center for Nuclear Physics (RCNP), Osaka University [6]. The average flux density of used neutron beam was  $2.17 \times 10^9 \text{ cm}^{-2} \text{ h}^{-1}$ . We obtained 63 SETs by measuring 26 of 31 fabricated test chips in 0.8 V operation for 18 hours.

We performed calibration by injecting a pseudo pulse to VDL through convergent OR cones. Using the calibration scheme explained in the previous section, we can obtain precise non-uniform time resolution of 230-stage VDL for each of 512 inverter chains in 26 test chips. However, we here calibrate only 63 pairs of VDL and inverter chains in which SETs occurred

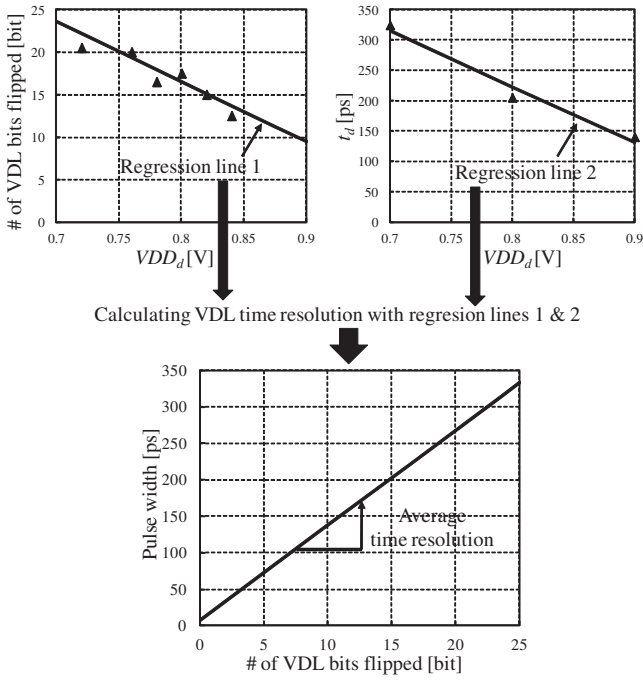


Fig. 9. An example of calculating a VDL time resolution by using two regression lines through the assessed pulse-width (which equals to  $t_{d1}$ ) and the calibrated VDL outputs.

for the sake of simplicity and obtain 63 variations of VDL time resolution.

Figure 9 exemplifies the calculation of VDL time resolution used in this paper. We here evaluated VDL outputs by sweeping  $VDD_d$  of on-chip pulse generator, and obtained the relation between the number of flips in the VDL latch chain and  $VDD_d$ . Furthermore, we assessed the propagation delay of the delay element  $t_d$ , which equals to the width of injected pseudo pulse, at different voltages. We then obtain two regression lines; VDL outputs versus  $VDD_d$  and  $t_d$  versus  $VDD_d$ . From these two regression lines, we finally calculated the VDL time resolution for a converging path on a chip. This calibration was carried out for 63 converging paths on different chips. Note that the non-uniform time resolution within a VDL, which originates from within-die variation, is ignored in this calibration procedure.

Figure 10 depicts the calibrated pulse-width distribution in 10 ps time resolution. The time range and average pulse-width of measured SETs are 5 ps to 215 ps and 67 ps, respectively. With the current calibration procedure, some of measured SETs might be underestimated because of the regression in Figure 9. The calibration that explicitly considers non-uniform time resolution of VDL is a future work. However, the measured SET widths are obviously narrower than those of several former results which used a long combinational logic chain, e.g. the average pulse-width is about 600 ps in [7] which used a chain of 1,000 minimum-drive-strength inverters in 90 nm process. This tendency is consistent with recent results [3, 8]. The pulse-width modulation must be carefully eliminated for SET pulse-width characterization.

On the other hand, Figure 11 shows the pulse-width distribution calculated with the uniform VDL time resolution obtained by circuit simulation. The time range and average pulse-width

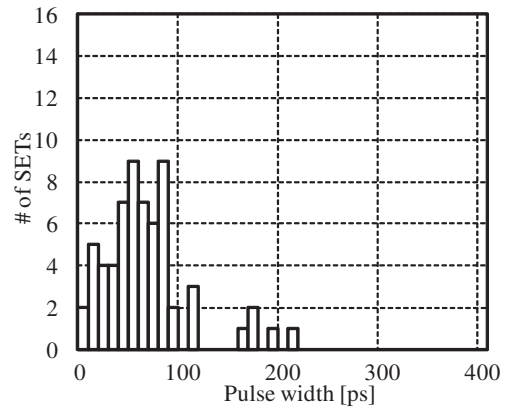


Fig. 10. Calibrated pulse-width distribution of 63 SETs depicted in 10 ps time resolution. Time range and average pulse-width of measured SETs are 5 ps to 215 ps and 67 ps, respectively.

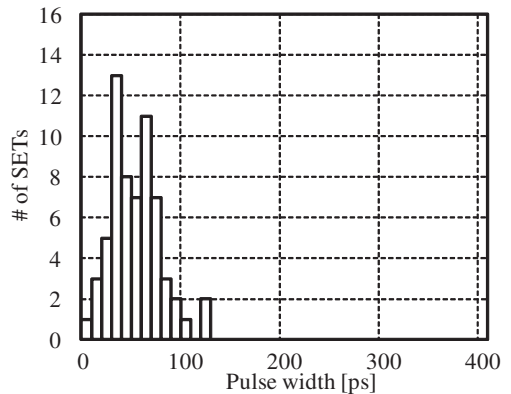


Fig. 11. Pulse-width distribution obtained by applying simulated time resolution of 4.8 ps to measured SETs. Time range and average pulse-width of measured SETs are 9 ps to 126 ps and 54 ps, respectively.

of measured SETs are 9 ps to 126 ps and 54 ps, respectively. Clearly, the calibrated pulse-widths of Figure 10 are widely distributed compared to non-calibrated ones of Figure 11. While the difference in average pulse-width between two situations is not significant, the difference in maximum pulse-width may cause unexpected reliability degradation. For example, when a delay element of 126 ps is inserted into BISER [9] to filter out all SETs, 7.9 % of measured SETs cannot be filtered out and actually propagate to FFs, which may cause failures. This manifests the importance of calibration for SET pulse-width distribution.

#### IV. DISCUSSION

Figure 12 shows the histogram of VDL time resolution after calibration. The time resolution varies between 1.88 ps to 13 ps, and the average is 5.66 ps. A possible reason of such a large variation in VDL time resolution is the vulnerability of latches under within-die variation reported in [10], since the VDL was operating at 0.8V while the nominal voltage the foundry suggested is 1.2V. To achieve more robust VDL time resolution, the variation-tolerant FF design presented in [10] is necessary.

Because of die-to-die variation in VDL and die-to-die and within-die variations in the converging paths, without an appropriate calibration, we may misestimate pulse-width distribution. Let us show how the pulse-width distribution may vary depend-

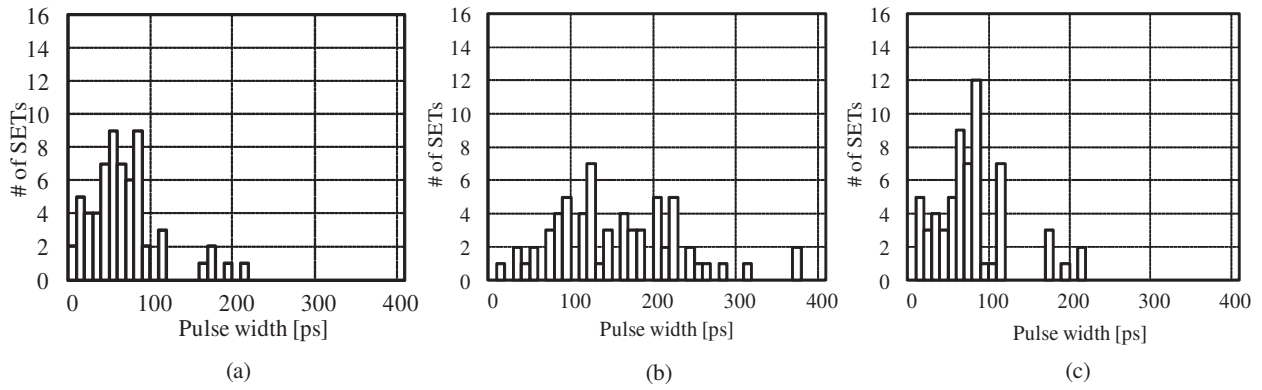


Fig. 13. Pulse-width distribution when applying a time resolution for a pair of VDL and converging path to other pairs of VDL and converging path: (a) the pulse-width distribution when applying the time resolution for each pair of VDL and converging path to the measured SETs propagating through each pair. (b) the pulse-width distribution when applying the coarsest time resolution of all pairs of VDL and converging path to all of measured SETs. (c) the pulse-width distribution when applying the coarsest time resolution of all pairs of VDL and converging path in each chip to the measured SET in each chip.

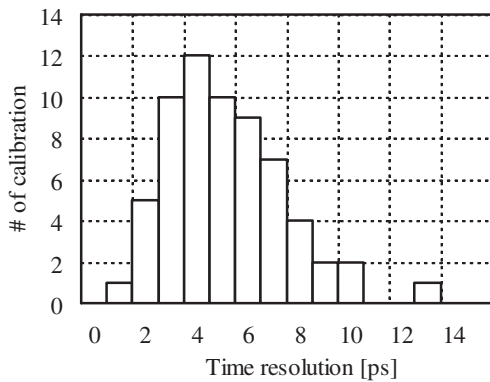


Fig. 12. The histogram of calibrated time resolution. Time range and average time resolution of this histogram are 1.88 ps to 13 ps and 5.66 ps, respectively.

ing on calibration approaches.

Figure 13 shows three pulse-width distributions with different calibration approaches listed below.

*Figure 13 (a):* within-die and die-to-die variation in the converging paths and die-to-die variation in VDL are eliminated using the calibration in the previous section. Thus, this figure is identical to Figure 10.

*Figure 13 (b):* The largest time resolution of 13 ps from 63 calibration results (Figure 12) is selected for calibration. In this case, within-die and die-to-die variation in the converging paths and die-to-die variation in VDL remain.

*Figure 13 (c):* die-to-die variation in the converging paths and VDL is eliminated. For each chip, a representative converging path is selected and its calibration result is used for the other converging paths on the same chip. In this experiment, the largest time resolution on the chip is chosen as the worst case. With this calibration approach, within-die variation in the converging paths remains.

Figure 13 (b) shows the widest pulse-width distribution when only a pair of the converging path and VDL is calibrated on a chip and the result is applied to the other pairs even on different chips. Time range and average pulse-width of this pulse-width distribution are 20 ps to 371 ps and 156 ps, respectively. This result clearly indicates the need for the post-

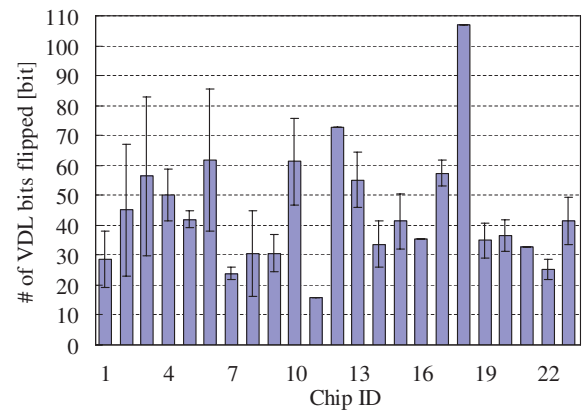


Fig. 14. VDL response of 23 calibrated chips to 200 ps pulse. Y-axis is the number of VDL bits flipped when capturing SET pulse.

fabrication calibration.

Next, Figure 13 (c) represents the widest possible pulse-width distribution when the calibration is performed only for a single converging path per chip. Time range and average pulse-width of this pulse-width distribution are 11 ps to 218 ps and 80 ps, respectively. Even after eliminating die-to-die variation, the average pulse-width could be overestimated by 19%. Furthermore, when looking at the overestimation of individual SET measurements, the maximum overestimation reaches 67 ps, for example 110 ps to 177 ps.

We finally show how the number of flips in VDL varies chip by chip even though the identical pulse is given. Figure 14 shows the VDL response of 23 chips in the case that the identical 200 ps pulse was injected. For each chip, about 3 converging paths were calibrated, and their averages and standard deviations of VDL bits are presented. Here, die-to-die variation changes the average, and within-die variation causes the standard deviation. We can see the range of  $\pm\sigma$  of chip 3 (26.5 bit) is comparable with, or rather, larger than the range of die-to-die  $\pm\sigma$  of all the chips (19.6 bit). This means calibration for die-to-die variation, which was carried out in [3], is not sufficient, and the effect of within-die variation should be eliminated as well.

## V. CONCLUSION

In this paper, we proposed a measurement circuit structure for capturing SET pulse-width suppressing pulse-width modulation and within-die variation of the measurement circuit. The proposed circuit uses parallelized short inverter chains as a target circuit to mitigate pulse-width modulation while maintaining area efficiency. Furthermore, each converging path and time-to-digital converter on each fabricated chip can be calibrated. Under neutron radiation, we observed narrow SET pulses whose width range is 5 ps to 215 ps. Calibration results also show that highly overestimated pulse-width distribution may be obtained when ignoring both variations, and point out that calibration for within-die variation of the measurement circuit is indispensable. As future works, we will evaluate non-uniform time resolution within a VDL and estimate its impact on SET pulse-width distribution.

## Acknowledgments

The VLSI chip in this study has been fabricated in the chip fabrication program of VLSI Design and Education Center (VDEC), the University of Tokyo in collaboration with STARC, e-Shuttle, Inc., and Fujitsu Ltd. The authors appreciate the support of Professor Kichiji Hatanaka and Assistant Professor Keiji Takahisa of Osaka University for the neutron radiation test at RCNP.

## REFERENCES

- [1] P. Shivakumar, M. Kistler, S.W. Keckler, D. Burger, and L. Alvisi, "Modeling the effect of technology trends on the soft error rate of combinational logic," in *Proc. DSN*, pp. 389–398, June 2002.
- [2] V.F. Cavrois, V. Pouget, D. McMorrow, J.R. Schwank, N. Fel, F. Essely, R.S. Flores, P. Paillet, M. Gaillardin, D. Kobayashi, J.S. Melinger, O. Duhamel, P.E. Dodd, and M.R. Shaneyfelt, "Investigation of the propagation induced pulse broadening (PIPB) effect on single event transients in SOI and bulk inverter chains," *IEEE Trans. on Nucl. Sci.*, vol.56, no.4, pp. 2014–2020, Aug. 2009.
- [3] J. Furuta, C. Hamanaka, K. Kobayashi, and H. Onodera, "Measurement of neutron-induced SET pulse width using propagation-induced pulse shrinking," in *Proc. IRPS*, pp. 5B.2.1–5B.2.5, Apr. 2011.
- [4] B. Gill, N. Seifert, and V. Zia, "Comparison of alpha-particle and neutron-induced combinational and sequential logic error rates at the 32nm technology node," in *Proc. IRPS*, pp. 199–205, Apr. 2009.
- [5] R. Harada, Y. Mitsuyama, M. Hashimoto, and T. Onoye, "Measurement circuits for acquiring SET pulse width distribution with sub-FO1-inverter-delay resolution," in *Proc. ISQED*, pp. 839–844, Mar. 2010.
- [6] Y. Tosaka, H. Ehara, M. Igeta, T. Uemura, H. Oka, N. Matsuoka, and K. Hatanaka, "Comprehensive study of soft errors in advanced CMOS circuits with 90/130 nm technology," in *Proc. IEDM Tech. Dig.*, pp. 38.3.1–38.3.4, Dec. 2004.
- [7] B. Narasimham, M.J. Gadlage, B.L. Bhuvu, R.D. Schrimpf, L.W. Massengill, W.T. Holman, A.F. Witulki, X. Zhu, A. Balasubramanian, and S.A. Wender, "Neutron and alpha particle-induced transients in 90 nm technology," in *Proc. IRPS*, pp. 478–481, Apr. 2008.
- [8] H. Nakamura, K. Tanaka, T. Uemura, K. Takeuchi, T. Fukuda, and S. Kumashiro, "Measurement of neutron-induced single event transient pulse width narrower than 100 ps," in *Proc. IRPS*, pp. 694–697, Apr. 2011.
- [9] S. Mitra, M. Zhang, N. Seifert, B. Gill, S. Waqas, and K.S. Kim, "Combinational logic soft error correction," in *Proc. ITC*, paper 29.2, Nov. 2006.
- [10] H. Sunagawa and H. Onodera, "Variation-tolerant design of D-flipflops," in *Proc. SOCC*, pp. 147–151, Sept. 2010.